Genetic characterization of the *Drosophila* homologue of *coronin*

V. Bharathi, S. K. Pallavi, R. Bajpai, B. S. Emerald and L. S. Shashidhara*

Centre for Cellular and Molecular Biology, Uppal Road, Hyderabad, India 500 007

*Author for correspondence (e-mail: shashi@ccmb.res.in)

Accepted 3 December 2003
Journal of Cell Science 117, 1911-1922 Published by The Company of Biologists 2004
doi:10.1242/jcs.01034

Summary

We report cloning and characterization of *coro*, which codes for the *Drosophila* homologue of the F-actin binding protein coronin. Viable alleles of *coro* produce a variety of phenotypes in leg, wing and eye development, which are similar to the phenotypes observed as a result of mutations in genes associated with the actin cytoskeleton and/or membrane trafficking. Homozygous lethal mutations in *coro* results in the disruption of the actin cytoskeleton in wing imaginal discs. Formation of both basolateral septate junctions and apical adherens junctions are also adversely affected in epithelial cells. Both viable and lethal alleles of *coro* show genetic interactions with *syntaxin1A*, a gene required for membrane trafficking. They also show enhanced response to over-expression of Decapentaplegic (Dpp) and its receptor Thick vein. Tracing of Dpp morphogen using a Dpp::GFP fusion construct suggested defects in the endocytic pathway, which resulted in uniform distribution of Dpp along the AP axis rather than a gradient from the AP boundary. Our results provide a genetic link between endocytosis/exocytosis events involving F actin-coated vesicles and the establishment of morphogen gradient.

Key words: Coronin, *Drosophila melanogaster*, Anteroposterior boundary, Dpp signaling, Membrane trafficking

Introduction

The actin cytoskeleton and associated proteins play many important roles both during development and during normal function of a differentiated cell. They are required for cell shape control, cortical stiffness/tension, spindle rotation, cytokinesis, cell and nuclear migration, vesicle and organelle transport, transport of morphogens and other cell fate determinants. Reorganization of the cytoskeleton, in particular actin polymerization, is the driving force for epithelial cell-cell adhesion (Vasioukhin et al., 2000; Vasioukhin and Fuchs, 2001). Very often microtubule and actin filament networks cooperate functionally during cellular processes such as transport of vesicles and organelles (Goode et al., 2000). Understanding the biochemical mechanisms that control the organization of actin is thus important and has implications for health and disease.

Amongst the many actin-associated proteins that mediate various functions of the actin cytoskeleton, the coronin family of proteins is highly conserved: from *Dictyostelium* to human. They are known to promote actin polymerization, cytokinesis and all actin-mediated processes (de Hostos et al., 1993) (for a review, see de Hostos, 1999). Analyses of coronin-GFP (green fluorescent protein) fusions and knockout mutants show that coronin participates in the remodeling of the cortical actin cytoskeleton that is responsible for phagocytosis and macropinocytosis (Maniak et al., 1995; Hacker et al., 1997). Likewise, in mammalian neutrophils, a coronin-like protein is associated with the phagocytic apparatus (Grogan et al., 1997). In addition to their association with proteins such as vinculin at focal contacts, they are also part of the actin cross-bridge between the actin cytoskeleton and the plasma membrane (Nakamura et al., 1999). Establishment of anterior-posterior (AP) polarity in the *Caenorhabditis elegans* embryo depends on POD-1, a coronin-like protein. Loss of POD-1 from early embryos results in a loss of physical and molecular asymmetries along the AP axis (Rappleye et al., 1999). It also causes the formation of large vesicles of endocytic origin, membrane protrusions, unstable cell divisions, a defective eggshell and deposition of extracellular material (Rappleye et al., 1999). Human coronin protein (TACO) is involved in the survival of mycobacteria and *Helicobacter pylori* in phagosomes (Ferrari et al., 1999; Zheng and Jones, 2003). TACO is actively retained on the outer surface of the phagosomes by living mycobacteria and thereby prevents their delivery to lysosomes, allowing mycobacteria and *Helicobacter pylori* to survive within macrophages. It has been further shown that cholesterol mediates the phagosomal association of TACO (Gatfield and Pieters, 2000). By entering host cells at cholesterol-rich domains of the plasma membrane, mycobacteria may ensure their subsequent intracellular survival in TACO-coated phagosomes.

We report cloning and characterization of *coro*, which codes for the *Drosophila* homologue of the F-actin binding protein coronin. Viable alleles of *coro* produce a variety of phenotypes in leg, wing and eye development, which are similar to the phenotypes observed as a result of mutations in genes associated with actin-cytoskeleton and/or membrane trafficking. Homozygous lethal mutations in *coro* results in the disruption of the actin cytoskeleton in wing imaginal discs. Formation of both basolateral septate junctions and apical adherens junctions are adversely affected in the epithelial cells of these strong alleles. Both viable and lethal alleles of *coro* show genetic interactions with *syntaxin1A* (*syx1A*), a gene

required for membrane trafficking. They also show enhanced response to Decapentaplegic (Dpp) and its receptor Thickvein (Tkv) over-expression. Tracing of Dpp morphogen using a Dpp::GFP fusion construct suggested uniform distribution of Dpp along the AP axis rather than a gradient from the AP boundary. In addition, over-expression of Dpp restored the normal actin cytoskeleton, which supports earlier finding on the role of Dpp in cytoskeletal regulation. These results on cloning and characterization of *coro*, thus, provide a new tool to employ the power of *Drosophila* genetics to understand the role of the actin cytoskeleton in various developmental processes.

Materials and Methods

Standard genetic techniques were used for balancing excision mutations, making recombinant chromosomes and combinations of different mutations and/or markers. 409-GAL4 was identified in the lab in a screen for enhancer-traps to identify targets of homeotic gene function. Polytene chromosome in situ hybridization, plasmid rescue and sequencing of the flanking genomic DNA were carried out as per the standard protocols. Excision mutations were generated by crossing 409-GAL4 to a genetic source of transposase. UAS lines used in this study were, UAS-lacZ (Brand and Perrimon, 1993), UAS-GFP (Lee and Luo, 2001), UAS-Dpp::GFP (Teleman and Cohen, 2000), UAS-activated Thickvein (UAS-Tkv*) (Nellen et al., 1996) and dominant negative form of Syntaxin1A (UAS-DNsyx1A; SKP and LSS, unpublished). *omb*-lacZ is described by Tsai et al. (Tsai et al., 1997) and *dpp*-GAL4 by Morimura et al. (Morimura et al., 1996). UAS-DNsyx1A is an EP insertion within the transcribed region (800 bp from the transcription start site) of *syx1A*. It was isolated in an EP screen using *Ubx*-GAL4 driver (Pallavi and Shashidhara, 2003) to identify suppressors and enhancers of *Ubx* (S.K.P. and L.S.S., unpublished). RT-PCR analysis confirmed that this EP line expresses a truncated transcript. In all tissues, this EP insertion induced phenotypes that were identical to the phenotypes reported for loss of function alleles of *syx1A* (Shulze and Bellen, 1996), thus suggesting that it expresses a dominant negative form of Syx1A.

Histology

RNA in situ hybridization was done essentially as described by Tautz and Pfeifle (Tautz and Pfeifle, 1989) using cDNA clone LD32977 as the probe. X-gal staining and immunohistochemical stainings were essentially as described previously (Ghysen and O'Kane, 1989; Patel et al., 1989). Visualization of Dpp::GFP was as described by Teleman and Cohen (Teleman and Cohen, 2000). FITC-labeled actin-phalloidin was purchased from Molecular Probes, USA. The primary antibodies used were, anti-Arm (Riggleman et al., 1990) anti-Ci (Motzny and Holmgren, 1995), anti β-galactosidase (Sigma, St Louis, MO), anti-Dll (Vachon et al., 1992), anti-En (Patel et al., 1989), anti-FASIII (Patel et al., 1987), anti-Sal (Kuhnlein et al., 1994) and anti-Wg (Brook and Cohen, 1996). Anti-Arm, Anti-En, Anti-FasIII and anti-Wg antibodies were obtained from the Development Studies Hybridoma Bank, University of Iowa, USA. Confocal microscopy was carried out on a Meridian Ultima or on Zeiss LSM510/Meta microscope. Trypsin-mediated dissociation of imaginal disc cells was done according to the method of Neufeld et al., (Neufeld et al., 1998). The adult appendages were processed for microscopy as described previously (Shashidhara et al., 1999). For scanning electron microscopy (SEM), adult heads were air dried and coated with gold. SEM was carried out in an Hitachi S520 machine.

Results

Cloning of *coro*

In a GAL4-enhancer trap screen for segmentally modulated expression patterns, we identified a GAL4 insertion (409-GAL4), which showed segment-specific expression patterns in the embryonic CNS (V.B. and L.S.S., unpublished). The P-element insertion was mapped to polytene location 42C-D by in situ hybridization (data not shown). We cloned the genomic region adjacent to the site of the P-element insertion by plasmid rescue and sequenced the same. The 409-GAL4 enhancer-trap insertion was mapped to the 5′ (at bp 56) untranslated region of CG9446 a predicted gene within AE003790 with considerable homology to coronin family of proteins (hereafter referred to as Coro). At the genomic level, the insertion was at position 82185 bp of AE003790, the genomic contig from the 42C8 region of the polytene chromosome (as per the BDGP Release 1.0; http://www.fruitfly.org; Fig. 1A).

By northern blot analysis, we identified a single species of transcript of size ~2.5 kb (Fig. 1B). Amongst the many cDNA clones from BDGP EST collection, LD32977 is 2610 bp long. We completely sequenced this cDNA clone and it has been submitted to GenBank (accession no. AF467271). The transcription unit is 10443 bp long (as per the LD32977), consisting of seven exons and six introns (Fig. 1A). As per the BDGP Release 3.1, CG9446 transcript RA is 2941 bp long and the transcription unit is 10768 bp long. CG9446-RA is longer than LD32977 (and many other ESTs such as AT08250, RE67756, LD28262, RE30002, LD15561, RE13103, etc) by 70 bp at the 5′ end and by 260 bp at the 3′ end. The predicted translation product is 528 amino acid long (Fig. 1C), which is the same as the predicted protein of CG9446. The protein product has 2 WD repeats, which forms a β-propeller-like structure, believed to be important for coronin function (de Hostos, 1999). At the C-terminal end it has a α-helical coiled coil domain (Fig. 1D), a dimerization domain, which is implicated in its localization to cell periphery (Asano et al., 2001).

It shows considerable identity at the protein sequence level to a number of coronin and coronin-like proteins from different organisms across the entire eukaryotic spectrum – from yeast to human (http://flybase.bio.indiana.edu/.bin/fbidq.html, FBgn0033109). Its closest homologues are coronins from mosquito (74% identity across 376 residues) and zebrafish (55% identity across 265 residues), followed by human, *Xenopus*, mouse and rat (around 54% identity across 265 residues), in that order.

Coro is expressed in all cells

The 409-GAL4 enhancer-trap driver showed a tissue-specific expression pattern. In imaginal discs its expression is restricted to only the peripodial membrane (Fig. 2A). More than 100 ESTs have been identified for *coro* from a number of different cDNA libraries (such as LD, CK, AT, RE, RH, GM and SD libraries for embryonic, larval discs, adult head etc) from both BDGP and RIEKEN projects (http://www.fruitfly.org). This suggests that it is expressed in all tissues, probably at very high levels. Indeed, RNA in situ hybridization using the cDNA clone LD32977 suggested that *coro* is expressed in all cell types including differentiating embryonic CNS and differentiating photoreceptor neurons in eye discs (Fig. 2B-D,G-H). However, it is expressed at very low levels in the larval CNS (Fig. 2G). Recent report on the large-scale microarray analyses to determine gene expression during the life cycle of

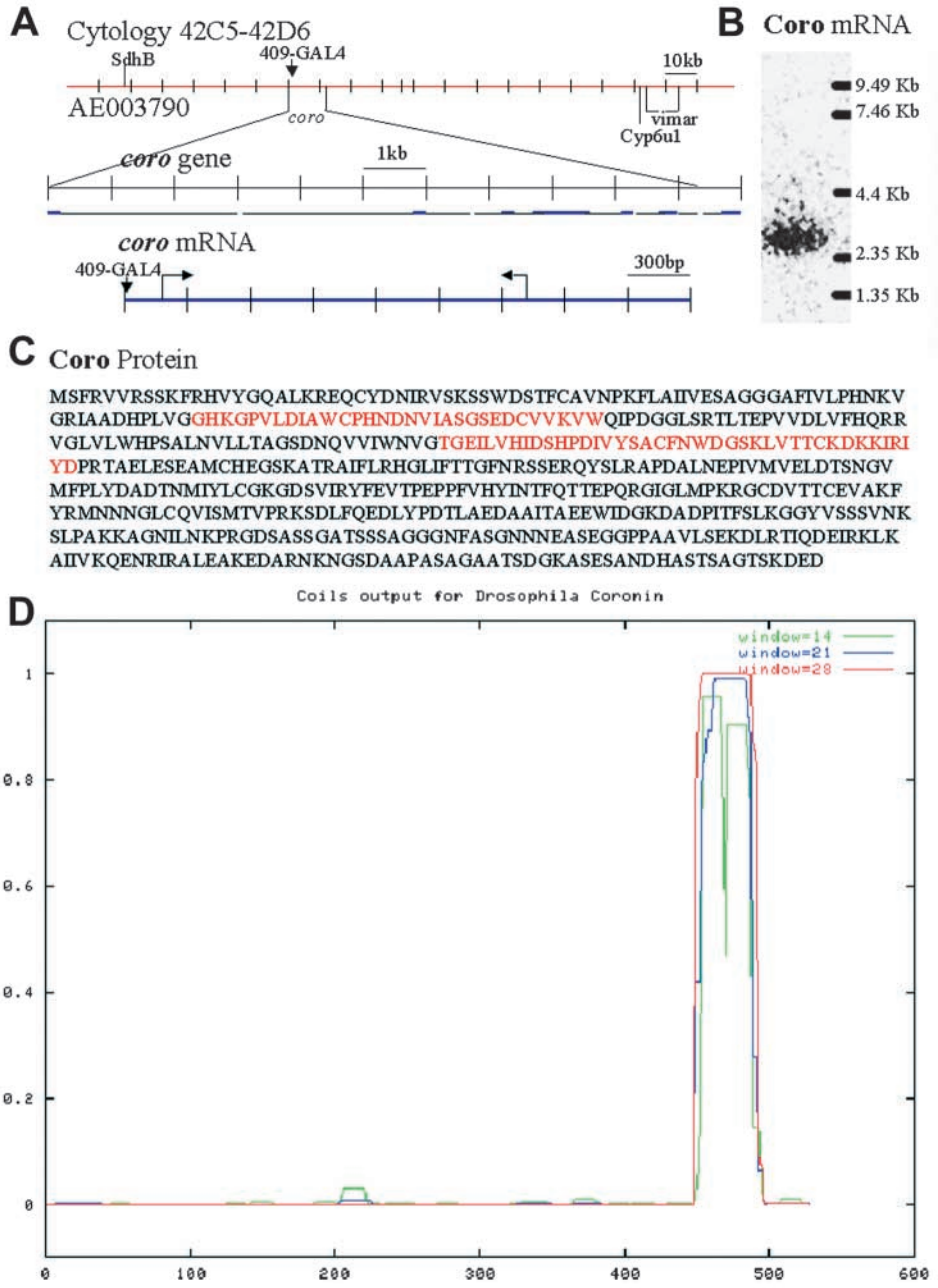

Fig. 1. (A) Genomic organization of the *coro* gene and the sequence of its protein product. Its cytological location is 42C5-D6. *coro* transcriptional length is 10443 bp, whereas the mRNA is 2610 nucleotides long. The P-element insertion in 409-GAL4 was in the 5′ UTR (within the first exon) of CG9446. (B) Northern blot showing a single Coro transcript of ~2.5 kb. (C) The predicted protein is 528 amino acids long, with 2 distinct WD40 repeats, shown in red. (D) Predicted coiled coil domain in the C-terminal of Coro protein. Predictions were carried out by submitting the protein sequence to BCM Search Launcher (http://searchlauncher.bcm.tmc.edu/seq-search/struc-predict.html).

Drosophila, suggests that Coro is expressed at very high levels at 0 hours AEL, suggesting a maternal contribution (Arbeitman et al., 2002). Its expression gradually comes down during embryogenesis, reaches lowest levels in the larval stages and rises again significantly in pupal stages.

Generation of mutations in *coro*

P-element insertion in the 409-GAL4 enhancer-trap line is within the 5′ UTR of *coro*. However, the strain is viable and did not show any abnormal phenotype. We generated deletion mutations within the *Drosophila coronin* gene by imprecise excision of the P-element. We generated six homozygous lethal and four partially viable mutations. All the ten alleles belong to a single complementation group. Amongst the six lethal excisions, five were early pupal lethal ($coro^{ex2}$, $coro^{ex3}$, $coro^{ex4}$, $coro^{ex6}$ and $coro^{ex7}$) and one ($coro^{ex8}$) was lethal at pharate adult stages. The viable alleles ($coro^{ex9}$, $coro^{ex10}$, $coro^{ex11}$ and $coro^{ex12}$) were lethal over the stronger alleles. All the alleles showed similar phenotypes in varying degrees of severity in homozygous and/or trans-allelic (trans-homozygous) combinations.

We used two representative alleles in all our experiments; $coro^{ex6}$ and $coro^{ex11}$. For these two alleles we did extensive polymorphism studies to identify the molecular nature of the mutation. First, we performed RT-PCR analyses to identify the nature of mutations. Since Coro is contributed maternally, we examined Coro transcripts in the third instar wing discs of homozygous $coro^{ex6}$ and $coro^{ex11}$ larvae. In $coro^{ex6}$, we detected a translocation of 231 bp from CG16791 of the third chromosome (cytology: 93C7) in the third exon of *coro* (Fig. 3A). Since we also noticed normal RT-PCR product, the translocated region may get spliced out, albeit inefficiently. We also designed primers to PCR-amplify genomic DNA flanking the site of the P-element insertion. In total 39 pairs of primers were designed to amplify 18 kb of genomic DNA as 500-800 bp long fragments from wild-type, homozygous $coro^{ex6}$ and $coro^{ex11}$ larvae. In addition to the translocation mentioned above, $coro^{ex6}$ showed a polymorphism at 1250 bp upstream of the transcription start site (Fig. 3A). Sequencing of this region indicated a 100 bp deletion. According to BDGP release 3.1, this region corresponds to the 3′ end of the predicted gene CG9447. Since no cDNA or EST clone is known for CG9447 (http://www.fruitfly.org), we attempted to examine if there is indeed a gene in this region. We designed two pairs of primers to amplify predicted exon1 alone and both exon1 and exon2. We did not see any amplification at the RT-PCR level (using RNA isolated from both embryos and larvae),

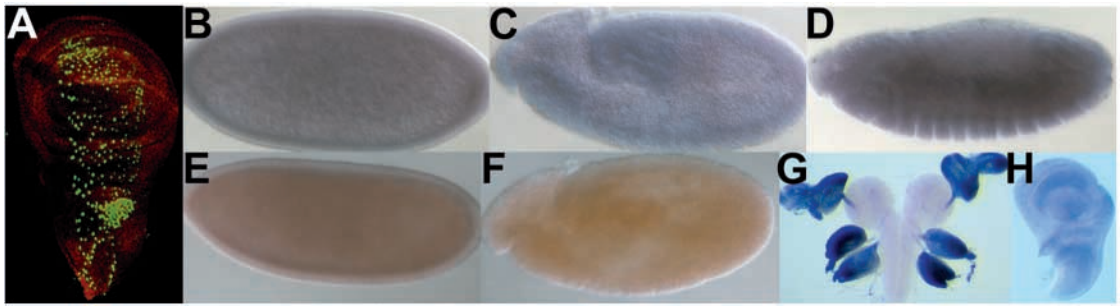

Fig. 2. Expression patterns of Coro transcripts. (A) The expression pattern of 409-GAL4 in wing discs revealed by UAS-nuclear *lacZ* (green). Note that 409-GAL4 is expressed only in the peripodial membrane. The disc proper is stained for Wingless (red). (B-D) Embryonic expression patterns of Coro. It is ubiquitously expressed in cellular blastoderm (B), extended germ band (C) and retracted germ band (D) stages. RNA in situ hybridization was done using antisense probes for LD32977. (E,F) Embryos of cellular blastoderm (E) and extended germ band (F) stages probed with sense RNA used as a negative control. (G-H) Post-embryonic expression patterns of Coro. It is expressed at high levels in eye, leg (G) and wing (H) imaginal discs. Note that it is expressed at very low levels in the larval CNS (G).

whereas these primers amplified products of expected sizes from the genomic DNA.

coro^{ex11} showed GAL4 activity (expression patterns were identical to that of original 409-GAL4), suggesting incomplete excision of the P-element. Similar GAL4 activity was noticed in two more alleles, *coro*^{ex8} and *coro*^{ex10}. Further PCR analyses indicated that they all have internal deletions of the P-element (thereby, removing w^+ activity). Northern blot analyses of RNA isolated from *coro*^{ex11} embryos showed two species of transcripts, one of normal size and the other longer. The longer transcript hybridizes to both LD32977 and GAL4 cDNA, suggesting a read-through transcript initiated at the P-element promoter (data not shown). Such read-through transcription initiated at the P-element promoter has been reported for *vg*^{2a33} allele of *vestigial* (Hodgetts and O'Keefe, 2001). We did not detect any other molecular lesion in the entire gene for *coro*^{ex11}.

Since all the excision alleles belonged to one complementation group, all show identical phenotypes (although with varying degree of severity) and, at least four alleles (*coro*^{ex6}, *coro*^{ex8}, *coro*^{ex10} and *coro*^{ex11}) show molecular lesion in *coro*; the observed phenotypes are due to mutations in the *coro* locus. Furthermore, analyses of wing disc mRNA suggest that both the alleles selected are regulatory in nature.

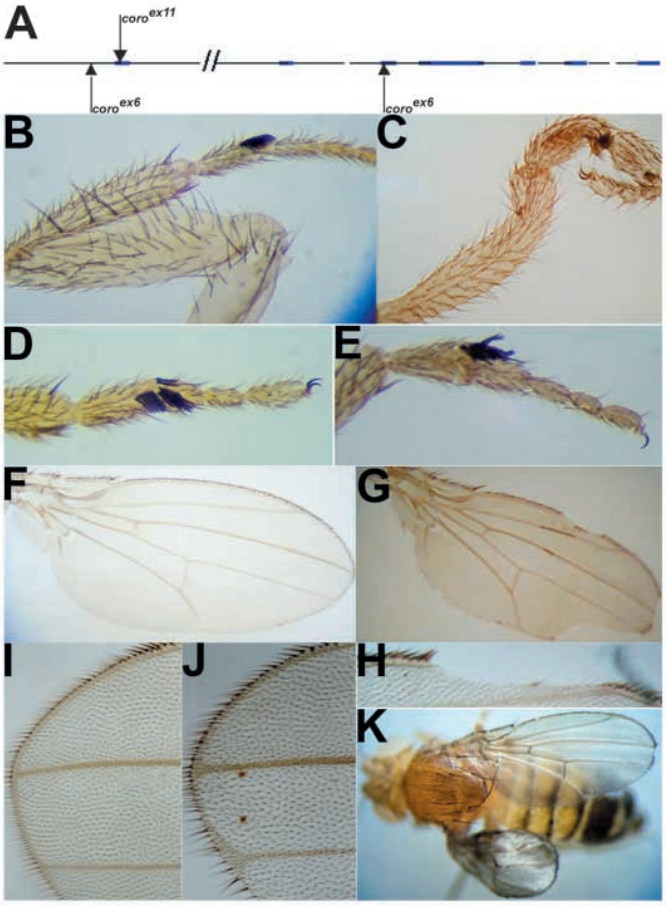

Mutations in *coro* affect adult morphogenesis

Homozygous *coro*^{ex11} is lethal at early to late pupal stages. Viability is 10%, although all homozygous female flies are sterile. The ovary in these flies is very small and devoid of any oocytes (data not shown). Homozygous *coro*^{ex11} flies exhibited a variety of leg, wing and eye phenotypes. Legs of *coro*^{ex11} flies appeared to be short and thick (Fig. 3C). We observed duplication of sex combs (Fig. 3D,E), an indication of ventralization of legs. However, we did not observe any altered phenotype at the levels of Wingless (Wg), Dpp and Distal-less (Dll) expression patterns (data not shown). The trans-alleleic combination *coro*^{ex6}/*coro*^{ex11} pharate adults often showed total

Fig. 3. Leg and wing phenotypes displayed by homozygous *coro*^{ex11} flies. (A) Molecular lesions in *coro*^{ex11} and *coro*^{ex6} alleles. *coro*^{ex11} carries a P-element insertion at the 5′UTR. *coro*^{ex6} has a 100 bp deletion in the upstream regulatory region and a translocation within the third exon. (B) Wild-type leg. (C-E) *coro*^{ex11}/*coro*^{ex11} legs. Note shortening and thickening of legs (C) and duplication of sex combs (D-E). (F) Wild-type wing blade. (G-H) Wing margin phenotypes seen in *coro*^{ex11}/*coro*^{ex11} flies. (G) Both anterior and posterior margins are affected. (H) The anterior margin defect at higher magnification. (I) Wild-type wing blade showing distal most region at higher magnification. (J) *coro*^{ex11}/*coro*^{ex11} wing blade. Note thickening of veins, which resembles the *Delta* phenotype, and small necrotic patches. (K) Adult *coro*^{ex11}/*coro*^{ex11} fly showing highly reduced wing blade.

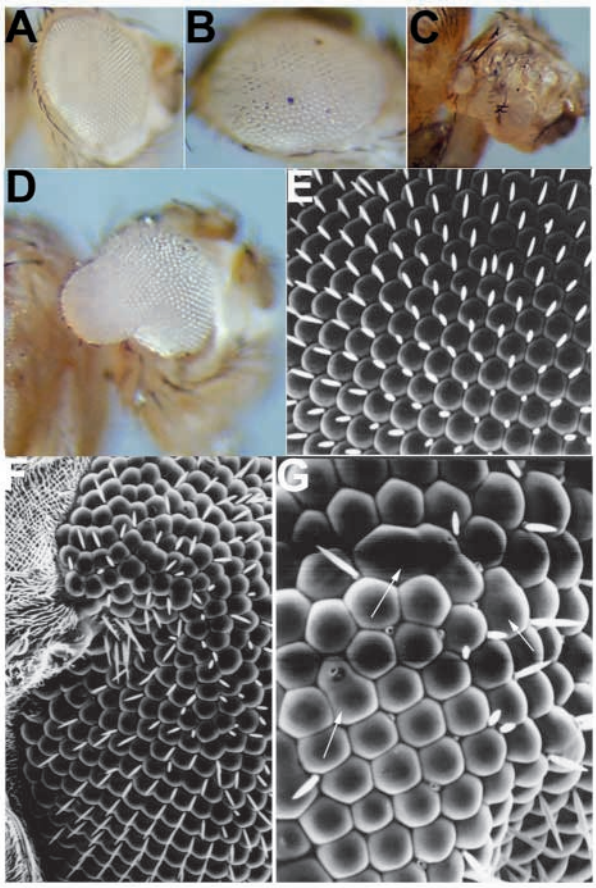

Fig. 4. Eye phenotypes of *coro* mutants. (A) Adult eye of w^{1118} flies. (B) Adult eye of a $coro^{ex11}/coro^{ex11}$ fly. Note rough-eye phenotype. (C) Total loss of eyes is often seen in $coro^{ex11}/coro^{ex11}$ flies. (D) $coro^{ex11}/coro^{ex11}$ fly showing loosely attached ommatidia, which are protruding anteriorly. (E) SEM image of wild-type eye showing regular array of ommatidia. (F,G) SEMs of $coro^{ex11}/coro^{ex11}$ eyes showing loss of ommatidia, fusion of ommatidia (arrows) and loss of inter-ommatidial bristles.

loss of one or more legs, which was more pronounced in segments T2 and T3 (data not shown). All $coro^{ex11}$ adult flies showed loss of anterior and/or posterior wing margin (Fig. 3G,H). They also showed thickening of veins and Delta vein phenotypes at the distal most regions (vein 3 and 4; Fig. 3J). Very often $coro^{ex11}$ flies showed a small-wing phenotype (Fig. 3K). They exhibited rough eye phenotypes (Fig. 4B,F) and often, total loss of eyes (Fig. 4C). They also showed lack of appropriate adhesion properties, which was reflected in loss of proper organization of ommatidia in the adult eye. We saw ommatidia loosely attached to each other, often protruding (Fig. 4D) and sometimes fused together (Fig. 4G).

coro mutants show disruption in actin cytoskeleton networks

The general appearance of all imaginal discs in $coro^{ex6}$, $coro^{ex11}$ and $coro^{ex6}/coro^{ex11}$ suggested that cells are loosely attached to each other. Trypsin (4.5 mg/ml) digestion of wing discs led to dissociation of $coro^{ex6}$ and $coro^{ex11}$ disc cells within 30-45 minutes, whereas wild-type wing discs took as long as 4 hours for complete dissociation of disc cells (Neufeld et al., 1998).

$coro^{ex11}$ wing discs stained with FITC-labeled actin-phalloidin showed marginal defects in the cytoskeleton (Fig. 5B). However, actin-phalloidin staining of $coro^{ex6}$ imaginal discs indicated that the actin-cytoskeleton is severely disrupted (Fig. 5C). The normal regular actin network was absent and we observed brightly stained spots, an indication that actin filaments are retracted and have formed actin-rich foci. One would predict that such severe disruption of the actin cytoskeleton in $coro^{ex6}$ discs would be lethal to cells. Indeed, $coro^{ex6}$ animals died at early pupal stages. Similar defects in the actin cytoskeleton were observed for $coro^{ex6}/coro^{ex11}$ wing discs (data not shown).

In both invertebrates and vertebrates, disruption in the actin cytoskeleton leads to loss of cell adhesion properties, particularly loss of adherens junctions (reviewed by Hall, 1998). For example, mutations in the small GTPase Rho, which regulates the actin cytoskeleton, affect DE-cadherin-based cell-cell adhesion in *Drosophila* embryos (Bloor and Kiehart, 2002). We therefore examined the effect of *coro* mutations on the expression of various markers of different spatial domains of epithelial cells. Along the apicobasal axis of epithelial cells, FITC-labeled actin-phalloidin, Armadillo (Arm) and *Drosophila* E-cadherin are localized at the apical end. Particularly, the latter two proteins label the site of the adherens junction, whereas antibodies to Discs large (Dlg), Fasciclin III (FasIII) and Coracle (Cor) label the more basal septate junctions (Woods, 1997). We observed moderate (in $coro^{ex11}$ wing discs) to severe (in $coro^{ex6}$ and $coro^{ex6}/coro^{ex11}$ wing discs) reduction in actin-phalloidin staining in the apical surface of epithelial cells (Fig. 5B,C). In both $coro^{ex6}$ and $coro^{ex6}/coro^{ex11}$ wing discs, Arm and FasIII were also reduced and very often show diffuse expression (data shown only for $coro^{ex6}$; Fig. 5E). Consistent with loss of actin-phalloidin staining, reduction in Arm levels was more severe than FASIII in both $coro^{ex11}$ (Fig. 5G) and $coro^{ex6}$ (Fig. 5H) discs. This by itself may not suggest loss of apicobasal polarity. Nevertheless, disruption in cell morphology is evident along the apicobasal axis, which is probably due to defective actin cytoskeleton.

Defective compartmental boundaries in *coro* mutant wing discs

Homozygous $coro^{ex11}$ wing discs are marginally smaller than wild-type discs. However, in as many as 30% (n=35) of $coro^{ex11}$ discs the anterior (A) and posterior (P) compartments are not properly joined along the AP boundary. They show a deep cleft along the AP boundary (Fig. 6B). Since animals showing such severe wing disc phenotypes were early pupal lethal, we could not ascertain corresponding adult wing phenotypes. Homozygous $coro^{ex6}$ wing discs do not show any such phenotypes in the AP or DV axes, probably because of severe defects in the actin cytoskeleton leading to cell death. Indeed, wing discs in $coro^{ex6}$ and a trans-alleleic combination $coro^{ex6}/coro^{ex11}$ are very small and often show total reduction of wing pouch area (Fig. 6C,D). A small number of $coro^{ex6}/coro^{ex11}$ wing discs did show a deep cleft along either AP or DV boundary (Fig. 6D).

Reduced viability of peripodial cells of the wing disc (caused by the suppression of Dpp signaling) causes similar

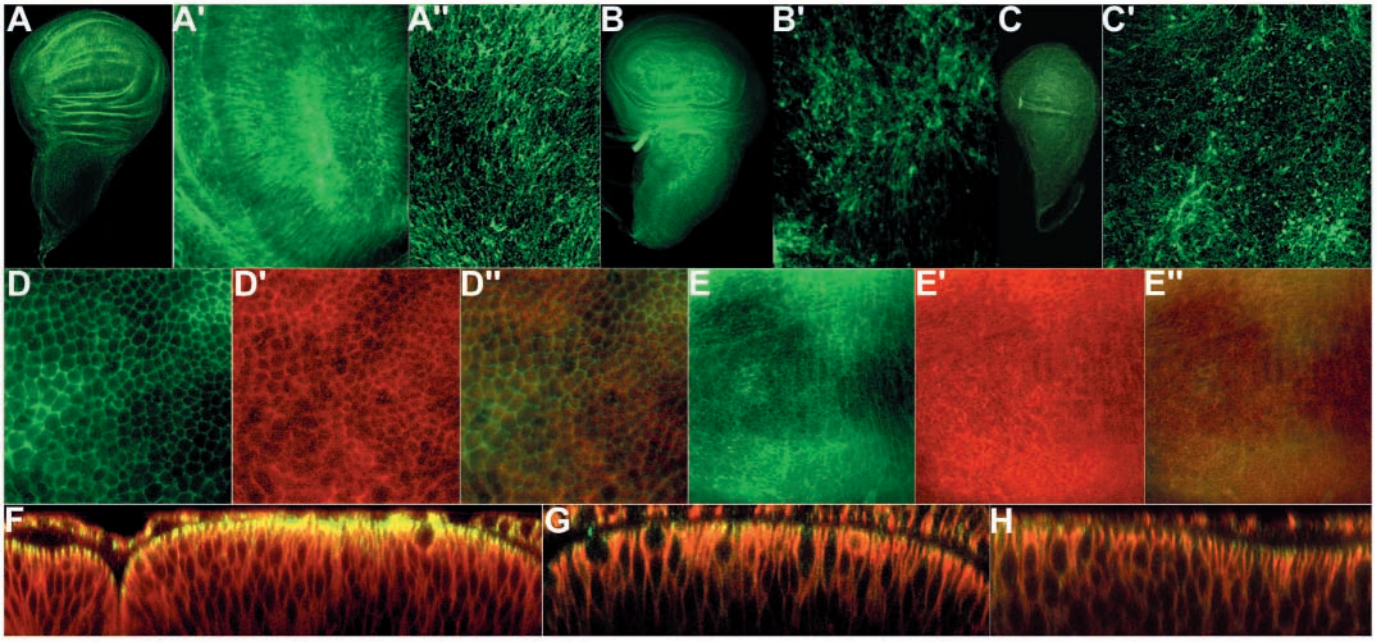

Fig. 5. Disruption of actin cytoskeleton and reduction in Arm and FASIII patterns along the apicobasal axis. (A-C) FITC-conjugated actin-phalloidin staining of wild-type (A), *coro*^{ex11}/*coro*^{ex11} (B) and *coro*^{ex6}/*coro*^{ex6} (C) wing discs. A′ and A″ show disc in A at higher magnifications. Similarly B′ and C′ are higher magnification images of discs shown in B and C, respectively. Note moderate to severe disruption of fine network of the actin cytoskeleton in B and C, respectively. *coro*^{ex6}/*coro*^{ex6} discs show a large number of darkly stained actin foci. Actin-phalloidin is normally localized to the apical surface of epithelial cells, which is reflected in higher intensity of staining at the DV boundary and at the presumptive hinge regions (A). In *coro*^{ex6}/*coro*^{ex6} discs, such intense staining of actin-phalloidin is lost (C) suggesting loss of actin-phalloidin from the apical surface. (D,E) Wild-type (D) and *coro*^{ex6}/*coro*^{ex6} (E) wing discs stained for Arm (green; D,E) and FASIII (red; D′,E′). D″ and E″ are the merged images of D and D′ and E and E′, respectively. Note that in *coro*^{ex6}/*coro*^{ex6} discs levels of both Arm and FASIII are very low and the staining is more diffused. (F-H) X-Z sections of wild-type (F), *coro*^{ex11}/*coro*^{ex11} (G) and *coro*^{ex6}/*coro*^{ex6} (H) wing discs stained for Arm (green) and FASIII (red). Note that normally Arm is apical and FASIII is basolateral. In wild-type wing discs both are expressed at very high levels. Both *coro*^{ex11}/*coro*^{ex11} and *coro*^{ex6}/*coro*^{ex6} show significant reduction in Arm and marginal reduction in FASIII staining indicating a possible defect in apicobasal polarity. In addition, cells are loosely arranged in *coro*$^{-}$ discs compared to wild-type disc, wherein cells are more compact. Normally *coro*^{ex6}/*coro*^{ex6} discs show severe loss of FASIII and Arm staining (as shown in E) and general loss of cell and disc morphology (as shown in C). To ascertain specific effects of loss of *coro* on apicobasal polarity of wing discs, we have chosen those *coro*^{ex6} wing discs, which show milder phenotype.

deep clefts along the AP and DV boundaries, more frequently in the AP boundary (Gibson et al., 2002). As mentioned above, 409-GAL4 is expressed only in the peripodial membrane (Fig. 2A). Since mutation in the *coro*^{ex11} strain is the result of incomplete excision of this P-element, we examined the viability and morphology of peripodial cells in *coro*^{ex11} wing discs. DAPI-stained wing discs did not reveal any effect on the viability of peripodial cells (data not shown). We stained the wing discs with Arm antibody, which outlines all cells. Large peripodial cells were examined using a laser scanning confocal microscope. The observed cleft along the AP boundary of *coro*^{ex11} wing discs was restricted to the disc proper and the peripodial membrane did not show any defect. Individual peripodial cells also appeared normal (Fig. 6F). Thus, formation of the cleft along the AP boundary may not be related to the reported dependence of disc growth on the viability of peripodial cells.

The observed cleft was always along the AP boundary. Either it is caused by enhanced cell-sorting between A and P cells or by defective AP boundary formation. Alternatively, the observed cleft could be the result of irregular Dpp signaling from the boundary, thus causing disproportionate growth between A and P compartments. The AP boundary is specified by the activity of Hedgehog (Hh), which diffuses from the P compartment to the A compartment to activate Dpp expression. In the presumptive AP boundary, Hh activates Cubitus interruptus (Ci) by stabilizing its full-length isoform, which in turn activates Dpp expression (reviewed by Aza-Blanc and Kornberg, 1999; Ingham and McMohan, 2001). Dpp signaling from the AP boundary is important for growth along the entire AP axis.

We examined possible patterning defects in *coro*^{ex11} wing imaginal discs at the levels of Engrailed (En), Ci and Dpp staining. We did not see any obvious defects in En (data not shown), Ci and Dpp expression patterns (Fig. 7B,D) in wing imaginal discs. This suggests that specification of the AP boundary is normal. In addition, expression patterns of DV markers such as Wg (Fig. 7F), Cut (Ct) and Dll in *coro*^{ex11} wing discs (data shown) were also normal.

Spalt (Sal) and Optomotor blind (Omb) are the two well-studied genes that respond to morphogenic activity of the Dpp gradient. In *coro*^{ex11} wing imaginal discs, we observed narrowing of the Sal expression domain in both anterior and posterior compartments; more severely in the latter compartment (Fig. 7H,I). Omb expression was also down regulated in the posterior compartment, while it was marginally

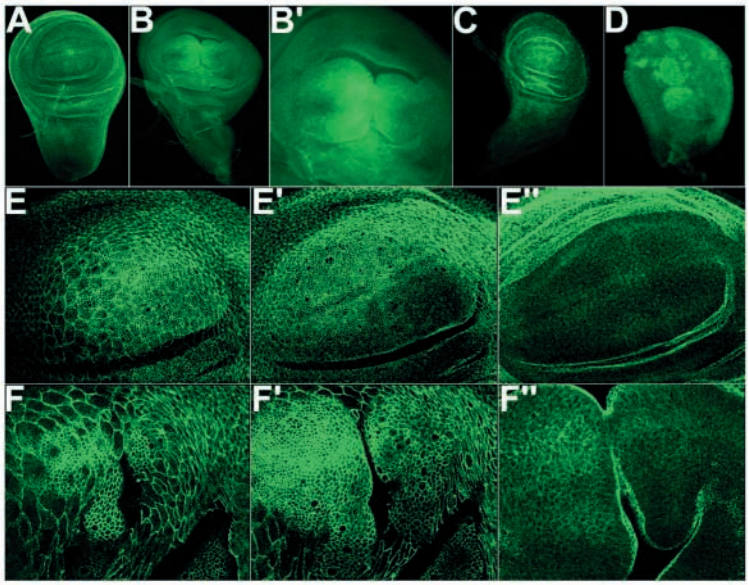

Fig. 6. *coro* mutant wing discs show defective AP boundary and reduced Dpp signaling to distant cells. (A) Wild-type wing disc. (B) $coro^{ex11}/coro^{ex11}$ wing disc showing separation of anterior and posterior compartments. (B′) Higher magnification image of the disc shown in B. (C) $coro^{ex6}/coro^{ex6}$ wing disc. Note that the disc is very small and no specific defect in the AP or DV boundary is seen. (D) $coro^{ex6}/coro^{ex11}$ wing disc. Note both small-disc phenotype as in $coro^{ex6}/coro^{ex6}$ discs and separation of dorsal and ventral compartments along the DV boundary. (E,E″) Optical sections of anti-Arm-stained wild-type wing disc to show that the epithelium is contiguous in all focal planes. (F,F″) Optical sections of anti-Arm-stained $coro^{ex11}/coro^{ex11}$ wing disc to show that peripodial membrane is contiguous and large squamous epithelial cells of the peripodial membrane are normal. Also in the disc proper, the columnar epithelium is contiguous, although mainly at the basal end of the cells. Images in E,E″ and F,F″ were generated by taking nearly 60 optical sections each of 0.5 μm thickness, which were then used to reconstruct disc images at three equal focal planes.

affected in the anterior compartment (Fig. 7K). These observations suggest down regulation of Dpp signaling to cells away from the AP boundary.

Enhanced response to Dpp over-expression in *coro* mutants

In flies, Dpp is transported from the source to recipient cells through a cycle of endocytosis and exocytosis of Dpp-containing vesicles (Gonzalez-Gaitan and Jackle, 1999; Teleman and Cohen, 2000; Entchev et al., 2000; Arquier et al., 2001). Furthermore, it is proposed that the balance between recycling and degradation of the ligand in the endocytic pathway determines the gradient of Dpp morphogen (Entchev et al., 2000). In *Dictyostelium*, coronin is required to regulate trafficking and fusion of actin-coated vesicles (Rauchenberger et al., 1997; Gotthardt et al., 2002). We therefore examined the dynamics of the Dpp gradient in *coro* mutant discs using a biologically active Dpp::GFP fusion protein (Teleman and Cohen, 2000). We over-expressed Dpp::GFP in the AP boundary (using a *dpp*-GAL4 driver) in wild-type and in *coro* mutant backgrounds. Surprisingly, *coro* mutant (both heterozygous and homozygous) discs over-expressing Dpp::GFP were much larger than wild-type discs over-expressing Dpp::GFP (Fig. 8B). Since $coro^{ex11}$ shows residual GAL4 activity, the phenotype in $coro^{ex11}$ and $coro^{ex6}/coro^{ex11}$ wing discs could be due to over-expression of Dpp::GFP in the peripodial cells. However, identical phenotypes were observed in the $coro^{ex6}$ background, which does not have any GAL4 activity of its own. Thus, the observed over-growth phenotype is caused by an enhanced response of *coro* mutant cells to Dpp::GFP over-expressed in the AP boundary.

In the wild-type background, Dpp::GFP forms an unstable gradient that spreads rapidly in the disc (Teleman and Cohen, 2000). Bright punctate spots of over-expressed Dpp::GFP are visible only in cells close to the AP boundary, the source of the protein (Teleman and Cohen, 2000; Entchev et al., 2000) (Fig. 8C). In addition, both brightness and number of spots per unit area decrease with the distance from the source, suggesting the formation of a gradient of Dpp::GFP. In $coro^{ex6}$

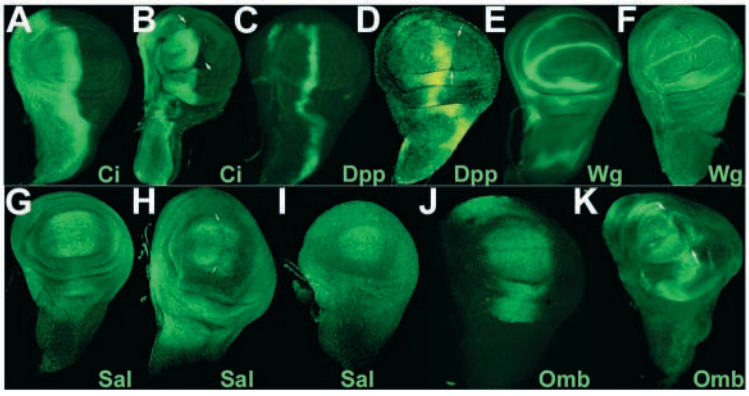

Fig. 7. Down regulation of Dpp signaling in *coro* mutants. (A,B) Ci expression patterns of wild-type (A) and $coro^{ex11}/coro^{ex11}$ (B) wing discs. Expression of Ci in $coro^{ex11}$ wing discs is normal, although they show defective AP boundary (arrows). (C,D) Expression pattern of Dpp in wild-type (C) and $coro^{ex11}/coro^{ex11}$ (D) wing discs. Dpp is visualized with the help of *dpp*-GAL4/UAS-GFP. In $coro^{ex11}/coro^{ex11}$ wing disc Dpp expression is normal despite separation of anterior and posterior compartments along the AP boundary (arrows). GFP seen in cells outside the AP boundary is mainly because of residual GAL4 activity of $coro^{ex11}$. (E,F) Wg expression patterns of wild-type (E) and $coro^{ex11}/coro^{ex11}$ (F) wing discs. Wg expression along the DV boundary is normal in the $coro^{ex11}$ wing disc. (G-I) Wild-type (G), $coro^{ex11}/coro^{ex11}$ (H) and $coro^{ex6}/coro^{ex6}$ (I) wing discs stained for Sal expression. Note reduced levels of Sal in $coro^{ex11}$ and $coro^{ex6}$ discs, particularly in the posterior compartment. Here too we have chosen those $coro^{ex6}$ wing discs that show milder phenotype, to examine the effect on Dpp signaling. (J-K) Wild-type (J) and $coro^{ex11}/coro^{ex11}$ (K) wing discs stained for Omb expression. Note that Omb expression in the posterior compartment is nearly absent.

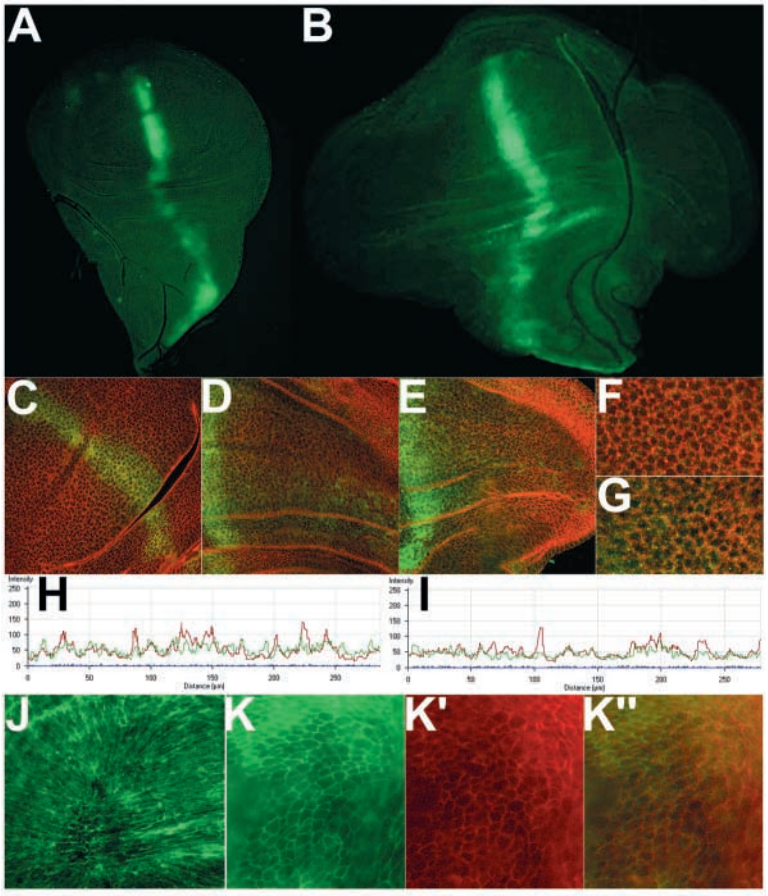

Fig. 8. Enhanced response to Dpp over-expression in *coro* mutants. (A,B) Low magnification images of *dpp*;GAL4/UAS-Dpp::GFP (A) and $coro^{ex11}/coro^{ex11}$; *dpp*;GAL4/UAS-Dpp::GFP (B) wing discs. Note differences in the size of the two discs. $coro^{ex11}$ and $coro^{ex6}$ heterozygous and $coro^{ex6}/coro^{ex6}$ and $coro^{ex6}/coro^{ex11}$ flies too showed enhanced growth response to Dpp-overexpression (data not shown). (C-E) Dpp::GFP-expressing wild-type (C), $coro^{ex11}/coro^{ex11}$ (D) and $coro^{ex6}/coro^{ex6}$ (E) wing discs stained for both GFP (green) and Arm (red). In the wild-type background, bright punctate spots of over-expressed Dpp::GFP are visible only in cells close to the AP boundary, the source of the morphogen. In *coro* mutant discs, bright spots of Dpp::GFP are visible in all cells of the disc, even in cells farthest from the AP boundary. (F,G) Dpp::GFP-expressing wild-type (F) and $coro^{ex11}/coro^{ex11}$ (G) wing discs shown at higher magnification. Note that in the $coro^{ex11}$ disc, bright spots of Dpp::GFP are larger, more numerous and mostly associated with the plasma membrane. (H,I) Intensity profile of wing discs shown in C and D, respectively. Posterior compartment cells immediately adjacent and parallel to the AP boundary were used for intensity profiling in both the discs. Note large number of Dpp::GFP peaks (green) outside Arm peaks (red) in wild-type background. However, nearly all DPP::GFP peaks coincide with Arm peaks in $coro^{ex11}/coro^{ex11}$ background suggesting that Dpp containing-vesicles are on the membrane. (J) $coro^{ex6}/coro^{ex6}$; *dpp*;GAL4/UAS-Dpp::GFP wing disc stained with FITC-conjugated actin-phalloidin. Note considerable rescue of actin cytoskeleton. Compare this disc with that of $coro^{ex6}/coro^{ex6}$ shown in Fig. 5C. (K) $coro^{ex6}/coro^{ex6}$; *dpp*;GAL4/UAS-Dpp::GFP wing disc stained with Arm (green) and FASIII (red). Note that the levels of both Arm and FASIII are now comparable to the wild-type (shown in Fig. 5D).

and $coro^{ex11}$ (both heterozygous and homozygous) and $coro^{ex6}/coro^{ex11}$ wing discs we observed bright spots of Dpp::GFP in all cells of the disc, even in cells farthest from the AP boundary (Fig. 8D,E). Dpp::GFP pattern appeared more uniform, suggesting that it has reached an equilibrium rather than a gradient with slopes on either side of the AP boundary. In addition, the size and number of bright spots of Dpp::GFP were higher in *coro* mutant discs than in wild-type discs (Fig. 8G). Since bright spots of Dpp::GFP represent a protease-resistant form of Dpp enclosed within endocytic vesicles (Teleman and Cohen, 2000; Entchev et al., 2000), it is possible that Dpp turnover is slowed down in *coro* mutant discs. Wing discs double stained for Arm showed that Dpp::GFP bright spots are not internalized in $coro^{-}$ wing discs (Fig. 8G,I). They remain on the cell membrane, mostly on the inside surface of the cells, suggesting defective membrane trafficking in $coro^{-}$ wing discs.

Interestingly, $coro^{ex6}/coro^{ex6}$ and $coro^{ex6}/coro^{ex11}$ discs over-expressing Dpp showed a partial rescue of the actin cytoskeleton and apicobasal polarity as visualized with actin-phalloidin, Arm and FasIII staining (Fig. 8J,K). This is consistent with the role of Dpp in maintaining the actin cytoskeleton (Harden et al., 1999; Ricos et al., 1999; Martín-Blanco et al., 2000). Dcdc42 and JNK and Dpp pathways interact to maintain the normal actin cytoskeleton during dorsal closure in embryogenesis (Harden et al., 1999; Ricos et al., 1999) and thorax closure during metamorphosis (Agnes et al., 1999; Martín-Blanco et al., 2000). Thus, these results suggest that severe loss of Dpp signaling could be the reason for defective active cytoskeleton associated with $coro^{ex6}$ discs. This correlates well with the fact that $coro^{ex6}$ animals die at late larval or early pupal stages (normally Dpp expression in wing discs is activated in late second/early third instar stages).

Over-expression of activated thickvein mimics coro phenotypes

Dpp is transported in endocytic vesicles, which would eventually be fused with lysosomes and degraded (Entchev et al., 2000). If Dpp turnover is slowed down in $coro^{-}$ wing discs because of impaired membrane trafficking and/or fusion with the lysosomes, it may lead to enhancement in Dpp signaling. If the amount of Dpp protein is a limiting factor, enhanced response would be seen only in the cells closer to the AP boundary, the source of the signal. The observed cleft along the AP boundary in homozygous $coro^{ex11}$ wing discs could therefore be due to enhanced Dpp signaling in the AP boundary. To examine this, we over-expressed activated the receptor of Dpp, Thickvein (Tkv*) using a *dpp*-GAL4 driver in wild-type and in *coro* mutant backgrounds. Interestingly, over-expression of Tkv* in the AP boundary of wild-type wing discs caused mild cleft formation along the boundary (Fig. 9A). Over-expression of Tkv* in $coro^{ex6}$ and $coro^{ex11}$ heterozygous backgrounds caused severe cleft phenotype with 85% penetrance (n=35) along the AP

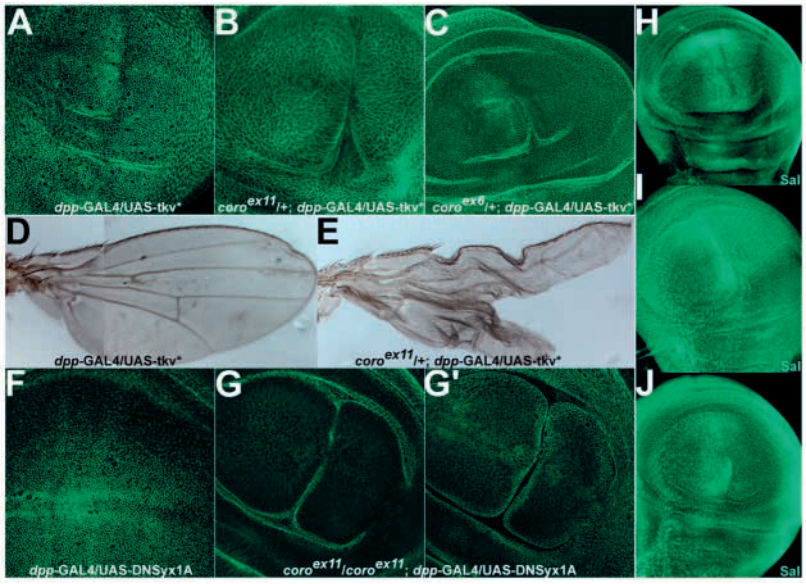

Fig. 9. Over-expression of activated Tkv mimics *coro* phenotypes. (A-C) *dpp*;GAL4/UAS-Tkv* (A), *coro*^{ex11}/+; *dpp*;GAL4/UAS-Tkv* (B) and *coro*^{ex6}/+; *dpp*;GAL4/UAS-Tkv* (C) wing discs stained for Arm to outline the cells. Over-expression of Tkv* in the AP boundary causes cleft formation similar to that in *coro*$^{-}$ discs (Fig. 6B), although the phenotype is milder. Over-expression of Tkv* in *coro*^{ex6} and *coro*^{ex11} heterozygous backgrounds, however, results in the formation of a deep cleft, which is normally seen in *coro*^{ex11} homozygous background (Fig. 6B). Over-expression of Tkv* in *coro*^{ex6} and *coro*^{ex11} homozygous backgrounds caused very high levels of lethality in early larval stages. (D,E) Adult wing blades of *dpp*;GAL4/UAS-Tkv* (D) and *coro*^{ex11}/+; *dpp*;GAL4/UAS-Tkv* (E) flies. Note severe notching of the wing blade in E. *coro*^{ex6}/+; *dpp*;GAL4/UAS-Tkv* also showed similar phenotypes. (F,G) *dpp*-GAL4/UAS-DNSyx1A (F) and *coro*^{ex11}/*coro*^{ex11}; *dpp*-GAL4/UAS-DNSyx1A (G) wing discs stained for Arm to outline the cells. Over-expression of DN-Syx1A in the AP boundary does not cause any significant phenotype. The severity and penetrance of cleft phenotype is enhanced when DN-Syx1A is expressed in *coro*^{ex11} background. G and G′ show two different levels of optical sections. *coro*^{ex6} over-expressing DN-Syx1A were lethal at early-third instar larval stages and therefore we were unable to examine third instar wing discs. (H,I) *dpp*;GAL4/UAS-Tkv* (H), *coro*^{ex11}/+; *dpp*;GAL4/UAS-Tkv* (I) and *coro*^{ex6}/+; *dpp*;GAL4/UAS-Tkv* (J) wing discs stained for Sal. Over-expression of Tkv* causes down regulation of Sal in distant cells, which is more pronounced in the posterior cells (Lecuit and Cohen, 1998). Sal levels are severely reduced in both anterior and posterior cells when Tkv* is over-expressed in *coro* heterozygous backgrounds.

boundary of the wing disc (Fig. 9B,C). Enhancement of the *coro* phenotype was more pronounced in adult wing blades. Over-expression of Tkv* in the wild-type background caused defects in anterior cross-vein development; otherwise the wing blade is normal (Fig. 9D). Being recessive, *coro* heterozygous flies do not show any phenotype in any tissue, including wing blades (data not shown). However, over-expression of Tkv* in the *coro* heterozygous background caused a dramatic deep cleft along the AP boundary of wing blades (Fig. 9E). These results, therefore, suggest that cleft formation is indeed due to localized enhancement of Dpp signaling.

Loss of *syntaxin* enhances *coro* phenotypes

The above-mentioned results on accumulation of Dpp-containing vesicles in *coro*$^{-}$ discs and enhanced Dpp signaling in the AP boundary suggest a role for Coro in vesicle transport. Independent evidence on this line came from studies on genetic interactions between *coro* and *syx1A*. The adult wing phenotype (notching) and eye phenotypes (reduction in the number of ommatidia, fusion of ommatidia and protrusion of head cuticle into the region of eye proper) and rudimentary ovaries observed in *coro*^{ex11} are remarkably similar to the phenotypes reported for *syx1A* alleles (Shulze and Bellen, 1996). Syx1A interacts with other members of the SNARE (soluble NSF attachment protein receptor) complex in membrane trafficking and in particular, it is required for membrane fusion. F-actin, coronin and vinculin are all part of transport vesicles (Gotthardt et al., 2002). Interestingly, loss of POD-1 (homologue of coronin) in *C. elegans* causes accumulation of large vesicles of endocytic origin. We therefore, examined if *syx* genetically interacts with *coro*.

We used a dominant negative form of Syx1A (DN-Syx1A; see Materials and Methods) for localized removal of its function in wild-type and *coro* backgrounds. Over-expression of DN-Syx1A using *dpp*-GAL4 driver in the wild-type background does not cause any significant phenotype in wing discs (Fig. 9F). Its expression in both *coro*^{ex11} and *coro*^{ex6} homozygous background enhanced the lethality associated with these alleles, suggesting genetic interactions between the two genes. In the *coro*^{ex6} homozygous background, all the animals died at early third instar larval stage. Over-expression of DN-Syx1A in *coro*^{ex11} homozygous background also caused higher incidences (78%; n=17) of cleft formation along the AP boundary of the wing disc (Fig. 9G), suggesting that *coro* phenotype is enhanced by the loss of *syx1A*.

Sequestration of Dpp in *coro* mutant background

Although over-expression of Tkv* causes cell-autonomous enhancement of Dpp signaling, it sequesters Dpp, leading to loss of signaling in the neighboring cells. For example, over-expression of Tkv* in the AP boundary causes reduction in the Sal domain and limits its expression to the AP boundary (Lecuit and Cohen, 1998) (Fig. 9H). Similar down regulation of Sal is observed with *coro* alleles suggesting that in *coro*$^{-}$ discs Dpp is not transported to the distant cells, causing its sequestration within the AP boundary. Over-expression of Tkv* in the *coro*$^{-}$ background resulted in severe loss of Sal expression in both anterior and posterior cells distant to the AP boundary (Fig. 9I,J), which suggests stronger sequestration of Dpp.

To conclude, adult phenotypes, cytoskeletal defect in wing discs, a cleft along the AP boundary, enhanced response to Dpp signaling and accumulation of large Dpp-containing vesicles observed in *coro* mutants are all linked and the main cause appears to be the disruption of F-actin-coated vesicle trafficking and/or its fusion with the membrane.

Discussion

We have reported here the cloning and genetic characterization of the *Drosophila* homologue of coronin, a F-actin binding protein. The sequence analyses suggest that *coro* shares most features of coronin and coronin-like proteins. It has 2 WD repeats and an α-helical coiled coil domain at the C-terminal end. In the *coro* mutant background, we observed a number of phenotypes, such as disruption in actin networks and change in cell adhesion properties that are reported in the literature for loss of coronin function. Considering the very high sequence homology and similarities in loss-of-function phenotypes between *coro* and a number of other coronin genes from a range of species from *Dictyostelium* to human, suggest that *coro* is a functional homologue of coronin.

Our RNA in situ data suggests that Coro is expressed at high levels in all cells. This is further supported by the expression profile of *coro* during the life cycle of *Drosophila* as determined by Arbeitman et al. (Arbeitman et al., 2002). They carried out microarray-based gene expression studies of nearly one-third of all *Drosophila* genes, one of which is *coro*. Coro transcripts are seen at very high levels in 0-5-hour embryos – reflecting maternal contribution. Its expression is drastically reduced in 15-20-hour embryos and maintains a steady state level until pupal stages. A slight increase in transcript level has been observed in pupal stages. Very high levels of maternal contribution of *coro* transcript is reflected in the observations that all *coro* alleles are either early or late pupal lethal. Interestingly, Enabled (another actin binding protein) and Costa (a microtubule binding protein) show the highest correlation of expression to Coro (Arbeitman et al., 2002). Developmental stages at which these genes show higher levels of expression may be stages in which actin and microtubule structures play significant roles.

We have generated a number of *coro* alleles, both viable and lethal. Viable *coro* mutants displayed prominent wing and eye phenotypes. In addition, all homozygous females of viable alleles are sterile with severe defects in ovary development. These phenotypes are very similar to those reported for *syx1A* alleles (Shulze and Bellen, 1996). Furthermore, we have observed that down regulation of Syx1A in the AP boundary is sufficient to enhance the cleft phenotype observed in *coro*$^{-}$ discs. Syx1A is part of the SNARE complex and mediates membrane trafficking and fusion. Coronin protein (in *C. elegans* and *Dictyostelium*) is also required for vesicle transport (Rauchenberger et al., 1997; Rappleye et al., 1999). Although further biochemical investigations are required for confirmation, our genetic experiments suggest that *Drosophila* Coronin protein functions with Syx1A to mediate trafficking and fusion of F actin-coated vesicles.

Over-expression of Dpp::GFP (a fusion protein, which otherwise functions as normal Dpp) in the *coro*$^{-}$ background (either heterozygous or homozygous) caused a dramatic over-growth phenotype compared to its over-expression in wild-type wing discs. *coro* mutant wing discs over-expressing Dpp::GFP in the AP boundary showed large number of bright spots of GFP all along the AP axis suggesting more of Dpp in endocytic vesicles. Rapid turnover of Dpp is necessary to establish the morphogen gradient (Gonzalez-Gaitan and Jackle, 1999; Teleman and Cohen, 2000; Entchev et al., 2000). In *coro*$^{-}$ wing discs, either Dpp is not degraded or its degradation is slowed down, causing uniformly high levels of Dpp all along the AP axis and thereby causing the over-growth phenotype.

Wing discs heterozygous for *coro* mutations that were otherwise normal, showed high incidences of cleft formation when activated Tkv, the Dpp receptor in wing discs, was over-expressed in the AP boundary. This suggests that cleft formation is due to localized enhancement in Dpp signaling in the AP boundary. However, levels of Dpp targets in the cells distant to the AP boundary are down regulated in *coro* mutants, suggesting that Dpp is not transported to the distant cells. Enhanced Dpp signaling in the AP boundary, therefore, is attributed to its sequestration. The observed cleft along the AP boundary may reflect a fold caused by the overgrowth of anterior cells at the boundary and/or undergrowth of posterior cells.

However, over-expression of Dpp::GFP along the AP boundary (using *dpp*-GAL4 driver) caused enhanced growth all along the AP axis of *coro*$^{-}$ wing discs. Furthermore, we observed uniformly high levels of Dpp::GFP all over the *coro* mutant wing disc rather than a gradient, with high levels only in cells closer to the source of the signal. This appears to be contrary to the above-mentioned results, which suggested down regulation of Dpp signaling in cells away from the AP boundary. However, this may simply reflect the relative amounts of Dpp present in two genetic backgrounds. In *coro*$^{-}$ wing discs, the normal amount of Dpp is made in the AP boundary. If all of this Dpp is endocytosed, but not recycled because of defective exocytosis (and also not degraded since vesicles are not fused with the lysosomes for degradation) it may lead to sequestration of Dpp in the cells within and closer to the AP boundary. If the amount of Dpp protein was not a limiting factor (for example, when Dpp is over-expressed), there would be accumulation of Dpp in all the cells and as a consequence enhanced growth in the entire wing disc. The product of the *Drosophila* tumor suppressor gene *lethal (2) giant larvae* (*l(2)gl*) is required for the normal secretion of Dpp through exocytosis (Arquier et al., 2001). Similar to *coro*, *l(2)gl* is also required in the cytoskeleton for cell shape and polarity determination. In *l(2)gl* mutants too, slow turnover of Dpp could be the reason for the observed paradoxical over-growth phenotype. Finally, Dpp::GFP spots/speckles were always associated with the plasma membrane in *coro*$^{-}$ wing discs, whereas they were mostly inside the cells in wild-type wing discs. This suggests that Coro is required either for exocytosis (which recycles Dpp-containing vesicles) or for the fusion of endocytic vesicles with the lysosomes for protein degradation. Work (at cellular and biochemical levels) is in progress to determine if coronin is needed for vesicle recycling or for its degradation or both.

We thank the Bloomington Stock Center, Indiana, USA for generous supply of fly stocks, the Development Studies Hybridoma Bank, University of Iowa, USA for monoclonal antibodies and K. Basler and S. Cohen for providing us with various fly stocks and antibodies. We thank members of the lab for helpful discussions and the anonymous referees for suggestions to improve the manuscript. This work was supported by a grant from Department of Science and Technology (Government of India).

References

Agnes, F., Suzanne, M. and Noselli, S. (1999). The *Drosophila* JNK pathway

controls the morphogenesis of imaginal discs during metamorphosis. *Development* **126**, 5453-5462.

Arbeitman, M. N., Furlong, E. E. M., Imam, F., Johnson, E., Null, B. H., Baker, B. S., Krasnow, M. A., Scott, M. P., Davis, R. W. and White, K. P. (2002). Gene expression during the life cycle of *Drosophila melanogaster. Science* **297**, 2270-2275.

Arquier, N., Perrin, L., Manfruelli, P. and Sémériva, M. (2001). The *Drosophila* tumor suppressor gene *lethal(2)giant larvae* is required for the emission of the Decapentaplegic signal. *Development* **128**, 2209-2220.

Asano, S., Mishima, M. and Nishida, E. (2001). Coronin forms a stable dimer through its C-terminal coiled coil region: an implicated role in its localization to cell periphery. *Genes Cells* **6**, 225-235.

Aza-Blanc, P. and Kornberg, T. B. (1999). Ci: a complex transducer of the hedgehog signal. *Trends Genet.* **15**, 458-462.

Bloor, J. W. and Kiehart, D. P. (2002). *Drosophila* RhoA regulates the cytoskeleton and cell-cell adhesion in the developing epidermis. *Development* **129**, 3173-3183.

Brand, A. H. and Perrimon, N. (1993). Targeted gene expression as a means of altering cell fates and generating dominant phenotypes. *Development* **118**, 401-415.

Brook, W. J. and Cohen, S. M. (1996). Antagonistic interactions between wingless and decapentaplegic responsible for dorsal-ventral pattern in the *Drosophila* leg. *Science* **273**, 1373-1377.

de Hostos, E. L., Rehfuess, C., Bradtke, B., Waddell, D. R., Albrecht, R., Murphy, J. and Gerisch, G. (1993). Dictyostelium mutants lacking the cytoskeletal protein Coronin are defective in cytokinesis and cell motility. *J. Cell Biol*. **120**, 163-173.

de Hostos, E. L. (1999). The Coronin family of actin-associated proteins. *Trends Cell Biol.* **9**, 345-350.

Entchev, E. V., Schwabedissen, A. and González-Gaitán, M. (2000). Gradient formation of the TGF-β homolog Dpp. *Cell* **103**, 981-991.

Ferrari, G., Langen, H., Naito, M. and Pieters, J. (1999). A coat protein on phagosomes involved in the intracellular survival of mycobacteria. *Cell* **97**, 435-447.

Gatfield, J. and Pieters, J. (2000). Essential role of cholesterol in entry of mycobacteria into macrophages. *Science* **288**, 1647-1650.

Ghysen, A. and O'Kane, C. (1989). Neural enhancer-like elements as specific cell markers in *Drosophila*. *Development* **105**, 35-52.

Gibson, M. C., Lehman, D. A. and Schubiger, G. (2002). Lumenal transmission of Decapentaplegic in *Drosophila* imaginal discs. *Dev. Cell* **3**, 451-460.

González-Gaitán, M. and Jackle, H. (1999). The range of *spalt*-activating Dpp signalling is reduced in endocytosis defective *Drosophila* wing discs. *Mech. Dev.* **87**, 143-151.

Goode, B. L., Drubin, D. G. and Barnes, G. (2000). Functional cooperation between the microtubule and actin cytoskeletons. *Curr. Opin. Cell Biol.* **12**, 63-71.

Gotthardt, D., Warnatz, H. J., Henschel, O., Bruckert, F., Schleicher, M. and Soldati, T. (2002). High-resolution dissection of phagosome maturation reveals distinct membrane trafficking phases. *Mol. Biol Cell.* **13**, 3508-3520.

Grogan, A., Reeves, E., Keep, N., Wientjes, F., Totty, N. F., Burlingame, A. L., Hsuan, J. J. and Segal, A. W. (1997). Cytosolic phox proteins interact with and regulate the assembly of Coronin in neutrophils. *J. Cell Sci.* **110**, 3071-3081.

Hacker, U., Albrecht, R. and Maniak, M. (1997). Fluid-phase uptake by macropinocytosis in Dictyostelium. *J. Cell Sci.* **110**, 105-112.

Hall, A. (1998). Rho GTPases and the actin cytoskeleton. *Science* **279**, 509-514.

Harden, N., Ricos, M. G., Ong, Y. M., Chia, W. and Lim, L. (1999). Participation of small GTPases in dorsal closure: distinct roles for Rho subfamily proteins in epithelial morphogenesis. *J. Cell Sci.* **112**, 273-284.

Hodgetts, R. B. and O'Keefe, S. L. (2001). The mutant phenotype associated with *P*-element alleles of the *vestigial* locus in *Drosophila melanogaster* may be caused by a readthrough transcript initiated at the *P*-element promoter. *Genetics* **157**, 1665-1672.

Ingham, P. W. and McMahon, A. P. (2001). Hedgehog signaling in animal development: paradigms and principles. *Genes Dev.* **15**, 3059-3087.

Kuhnlein, R. P., Frommer, G., Friedrich, M., Gonzalez-Gaitan, M., Weber, A., Wagner-Bernholz, J. F., Gehring, W. J., Jäckle, H. and Schuh, R. (1994). spalt encodes an evolutionarily conserved zinc ϔnger protein of novel structure which provides homeotic gene function in the head and tail region of the *Drosophila* embryo. *EMBO J.* **13**, 168-179.

Lecuit, T. and Cohen, S. M. (1998). Dpp receptor levels contribute to shaping the Dpp morphogen gradient in the *Drosophila* wing imaginal disc. *Development* **125**, 4901-4907.

Lee, T. and Luo, L. (2001). Mosaic analysis with a repressible cell marker (MARCM) for *Drosophila* neural development. *Trends Neurosci*. **24**, 251-254.

Maniak, M., Rauchenberger, R., Albrecht, R., Murphy, J. and Gerisch, G. (1995). Coronin involved in phagocytosis: dynamics of particle-induced relocalization visualized by a green fluorescent protein tag. *Cell* **83**, 915-924.

Martín-Blanco, E., Pastor-Pareja, J. C. and Garciá-Bellido, A. (2000). JNK and *decapentaplegic* signaling control adhesiveness and cytoskeleton dynamics during thorax closure in *Drosophila*. *Proc. Natl. Acad. Sci. USA* **97**, 7888-7893.

Morimura, S., Maves, L., Chen, Y. and Hoffmann, F. M. (1996). *decapentaplegic* overexpression affects *Drosophila* wing and leg imaginal disc development and wingless expression. *Dev. Biol.* **177**, 136-151.

Motzny, C. K. and Holmgren, R. (1995). The *Drosophila* cubitus interruptus protein and its role in the wingless and hedgehog signal transduction pathways. *Mech. Dev.* **52**, 137-150.

Nakamura, T., Takeuchi, K., Muraoka, S. and Takezoe, H. (1999). A neurally enriched Coronin-like protein, ClipinC, is a novel candidate for an actin cytoskeleton-cortical membrane-linking protein. *J. Biol. Chem*. **274**, 13322-13327.

Nellen, D., Burke, R., Struhl, G. and Basler, K. (1996). Direct and long-range action of a DPP morphogen gradient. *Cell* **85**, 357-368.

Neufeld, T. P., de la Cruz, A. F., Johnston, L. A. and Edgar, B. A. (1998). Coordination of growth and cell division in the *Drosophila* wing. *Cell* **93**, 1183-1193.

Pallavi, S. K. and Shashidhara, L. S. (2003). Egfr/Ras pathway mediates interactions between peripodial and disc proper cells in Drosophila wing discs. *Development* **130**, 4931-4941.

Patel, N. H., Snow, P. M. and Goodman, C. S. (1987). Characterization and cloning of fasciclin III: a glycoprotein expressed on a subset of neurons and axon pathways in *Drosophila*. *Cell* **48**, 975-988.

Patel, N. H., Martin-Blanco, E., Coleman, K. G., Poole, S. J., Ellis, M. C., Kornberg, T. B. and Goodman, C. S. (1989). Expression of engrailed proteins in arthropods, annelids and chordates. *Cell* **58**, 955-968.

Rappleye, C. A., Paredez, A. R., Smith, C. W., McDonald, K. L. and Aroian, R. V. (1999). The Coronin-like protein POD-1 is required for anterior-posterior axis formation and cellular architecture in the nematode *Caenorhabditis elegans*. *Genes Dev*. **13**, 2838-2851.

Rauchenberger, R., Hacker, U., Murphy, J., Niewohner, J. and Maniak, M. (1997). Coronin and vacuolin identify consecutive stages of a late, actin-coated endocytic compartment in Dictyostelium. *Curr. Biol.* **7**, 215-218.

Ricos, M. G., Harden, N., Sem, K. P., Lim, L. and Chia, W. (1999). Dcdc42acts in TGF-β signaling during *Drosophila* morphogenesis: distinct roles for the Drac1/JNK and Dcdc42/TGF-β cascades in cytoskeletal regulation. *J. Cell Sci.* **112**, 1225-1235.

Riggleman, B., Schedl, P. and Wieschaus, E. (1990). Spatial expression of the *Drosophila* segment polarity gene *armadillo* is postranscriptionally regulated by *wingless*. *Cell* **63**, 549-560.

Sambrook, T., Fritsch, F. E. and Maniatis, T. (1989). *Molecular Cloning, A Laboratory Manual*. Cold Spring Harbor, NY: Cold Spring Harbor Laboratory Press.

Shashidhara, L. S., Agrawal, N., Bajpai, R., Bharathi, V. and Sinha, P. (1999). Negative regulation of dorsoventral signaling by the homeotic gene *Ultrabithorax* during haltere development in *Drosophila*. *Dev. Biol*. **212**, 491-502.

Schulze, K. L. and Bellen, H. J. (1996). *Drosophila* Syntaxin is required for cell viability and may function in membrane formation and stabilization. *Genetics* **144**, 1713-1724.

Tautz, D. and Pfeifle, C. (1989). A non-radioactive in situ hybridization method for the localization of specific RNAs in *Drosophila* embryos reveals translational control of the segmentation gene hunchback. *Chromosoma* **2**, 81-85.

Teleman, A. A. and Cohen, S. M. (2000). Dpp gradient formation in the *Drosophila* wing imaginal disc. *Cell* **103**, 971-980.

Tsai, S. F., Jang, C. C., Prikhod'ko, G. G., Bessarab, D. A., Tang, C. Y., Pflugfelder, G. O. and Sun, Y. H. (1997). Gypsy retrotransposon as a tool for the in vivo analysis of the regulatory region of the *optomotor-blind* gene in *Drosophila*. *Proc. Natl. Acad. Sci. USA* **94**, 3837-3841.

Vachon, G. B., Cohen, B., Pfeifle, C., McGuffin, M. E., Botas, J. and Cohen, S. (1992). Homeotic genes of the Bithorax complex repress limb

development in the abdomen of the *Drosophila* embryo through the target gene Distal-less. *Cell* **71**, 437-450.

Vasioukhin, V. and Fuchs, E. (2001). Actin dynamics and cell-cell adhesion in epithelia. *Curr. Opin. Cell Biol.* **13**, 76-84.

Vasioukhin, V., Bauer, C., Yin, M. and Fuchs, E. (2000). Directed actin polymerization is the driving force for epithelial cell-cell adhesion. *Cell* **100**, 209-219.

Woods, D. F., Wu, J. W. and Bryant, P. J. (1997). Localization of proteins to the apico-lateral junctions of *Drosophila* epithelia. *Dev. Genet.* **20**, 111-118.

Zheng, P. Y. and Jones, N. L. (2003). Helicobacter pylori strains expressing the vacuolating cytotoxin interrupt phagosome maturation in macrophages by recruiting and retaining TACO (Coronin 1) protein. *Cell Microbiol.* **5**, 25-40.